Journal of the Australian Ceramic Society (2018) 54:467–473
https://doi.org/10.1007/s41779-018-0173-8

RESEARCH

Effect of Mg doping on physical properties of Zn ferrite nanoparticles

Siva Kumar Pendyala[1,2] · K. Thyagarajan[3] · A. GuruSampath Kumar[4] · L. Obulapathi[5]

Received: 18 April 2017 / Revised: 12 December 2017 / Accepted: 11 January 2018 / Published online: 19 March 2018

Abstract

Effect of Mg doping on $ZnFe_2O_4$ samples was prepared by a sol-gel auto-combustion method. The obtained samples were sintered at different temperatures. Then, the sintered samples were characterized by powder X-ray diffraction, scanning electron microscopy, energy dispersive X-ray analysis, and electrical properties. XRD results confirm the formation of cubic spinel-type structure with an average crystallite size decreased with Mg concentration from 37 to 17 nm. Lattice parameter decreases with increasing Mg concentration, due to the small ionic radius of the Mg^{2+} ion. The SEM images show the morphology of the samples as spherical shaped particles in agglomeration. The magnetization showed an increasing trend with increasing Mg concentration due to the rearrangement of cations at tetrahedral and octahedral sites. The ionic conductivity is increased with the increase of Mg concentration.

Keywords Zn ferrite · Sol-gel auto-combustion method · Crystallite size · Dielectric behavior and ionic conductivity

Introduction

In recent years, researchers have been concentrating on improving the conductivity of nanocrystalline spinel ferrites by doping divalent metal cations. These nanocrystalline spinel ferrites are important materials due to having variety of properties like electrical and magnetic properties which are most useful in various applications such as microwave, gas sensors, and biomedical [1–4]. The $ZnFe_2O_4$ nanocrystalline spinel ferrites have been extensively studied by researchers worldwide, because of physical and chemical properties depending on their unique as compared to the bulk counterpart materials [5–7]. These ferrites are chemically and thermally stable and are suitable for a wide range of applications like magnetic materials, MRI (magnetic resonance imaging), drug delivery, and photocatalysts [8, 9]. Recently, Mg and Zn-based ferrites have attracted much attention due to its high electrical resistivity with good magnetic properties for transformers, ferrofluids, and magnetic cores. Mg-doped Zn ferrites have also been reported to be highly suitable for memory and switching circuits in digital computers and phase shifters [10]. These ferrites have been synthesized for their utilization in several microwave devices operating at L, S, and C bands [11]. Many researchers have been studied the potential applications of Mg-doped Zn ferrites in multilayer chip inductors, microwave, and hyperthermia [12–14].

In the present work, we have selected divalent Mg^{2+} as dopant because of its effective ionic radii. Furthermore, magnesium has low cost and high stability. The magnesium zinc ferrite compound is a soft ferrite [15]. Due to its useful properties in dielectric and magnetic applications, it is used in several applications like high-frequency range applications, as low hysteresis loss material, and high-density media storage, as recoding and sensor device [16, 17]. The divalent ions of magnesium and zinc are diamagnetic in nature. The distribution of these ions in the lattice sites may affect the properties of ferrites very much [18].

The synthesis of magnesium zinc ferrite has been reported by various chemical and solid state reaction methods. In this work, the dopant Mg in $ZnFe_2O_4$ system is varied from 0.2 to 0.6 M% ($Mg_xZn_{1-x}Fe_2O_4$ (0.2, 0.4 and 0.6 M% of MgO)) and

✉ Siva Kumar Pendyala
sampathkumar.physics@gmail.com;
sivakumarpendyala2015@gmail.com

1 Research Scholar, JNTUA, Anantapuramu, A.P. 515002, India

2 Department of Physics, Malla Reddy Engineering College (A), Secunderabad, T.S. 500100, India

3 Department of Physics, JNTUA College of Engineering, Pulivendula, A.P. 516390, India

4 College of Physics and Energy, Shenzhen University, Shenzhen 518060, People's Republic of China

5 Department of Physics, Annamacharya Institute of Tech. & Sci, Rajampet, A.P. 516126, India

is prepared by auto-combustion method. The structural parameters such as crystallite size, lattice parameters, grain size, and electrical properties were analyzed, and the influence of Mg on the same was explained.

Experimental details

Commercially available metal nitrates of magnesium nitrate ($Mg(NO_3)_2.6H_2O$), zinc nitrate ($Zn(NO_3)_2.6H_2O$) and ferric nitrate ($Fe(NO_3)_2.9H_2O$) (all are AR grade Sigma Aldrich, USA, 99.9% purity), citric acid were used as starting materials and ammonia is used as fuel material for this reaction. All these chemicals were mixed in an appropriate stoichiometric proportion by using the formulae $Mg_xZn_{1-x}Fe_2O_4$ (0.2, 0.4, and 0.6 M% of MgO). Auto-combustion method was used for the preparation of Mg-Zn ferrite. All the solutions were stirred well to get the homogeneous solutions. After mixing, the ratio of metal nitrates to citric acid was 1:3. These solutions were stirred continuously on 90 °C for 1 h by adding ammonia dropwise, so that the solution maintains pH value of 7. The resulting solution was evaporated by heating at about 150 °C on a hot plate with continuous stirring. The viscosity rose as a result of cross-linking of carboxylato-metal complexes into a three-dimensional structure and started to form a viscous gel. When finally all water molecules were removed from the mixture by increasing the temperature to 200 °C, the gel began frothing. The gel gave a fast flameless auto-combustion reaction with the evolution of large amounts of gases. It started in the hottest zones of the beaker and propagated from the bottom to the top like the eruption of a volcano. The reaction was completed in a minute giving rise to dark gray voluminous product with a structure similar to a branched tree. Finally, the burnt powder was ground and calcined in air at temperature of 500–1000 °C for 4 h to decompose of MgO and reground to obtain the spinel phase. A 2 mol% of polyvinylpyridine was added to the powder as binder and mixed thoroughly. The powder sample was uniaxially pressed by a pressure of 10 tons/in.^{2} to get disc-shaped pellets, and these pellets were sintered at 1400 °C for 2 h on air at slope of 2 C/min and cooled at room temperature of the same slope. Different characterizations were conducted for the prepared samples like XRD, SEM, EDAX, and electrical properties.

Results and discussion

XRD analysis

Figure 1 shows XRD patterns of Mg^{2+} (0.2, 0.4, and 0.6 M%) doped $ZnFe_2O_4$. These patterns confirm that compositions show the formation of cubic spinel-type structure (JCPDS card no. 22-1012) with an average crystallite size in the range of 15–50 nm [19]. All the samples show the presence of (111), (220), (311), (400), (422), (511), (440), and (533) diffraction peaks in the scanning range 20° to 80°. No other phases are detected in the Mg-doped $ZnFe_2O_4$ samples, which indicate that all the samples exhibit the single-phase cubic spinal structure. The average crystallite size of the samples is calculated from the diffraction peaks at (311), (440), and (511) planes in the XRD profile, in accordance with Debye–Scherrer formula [20]:

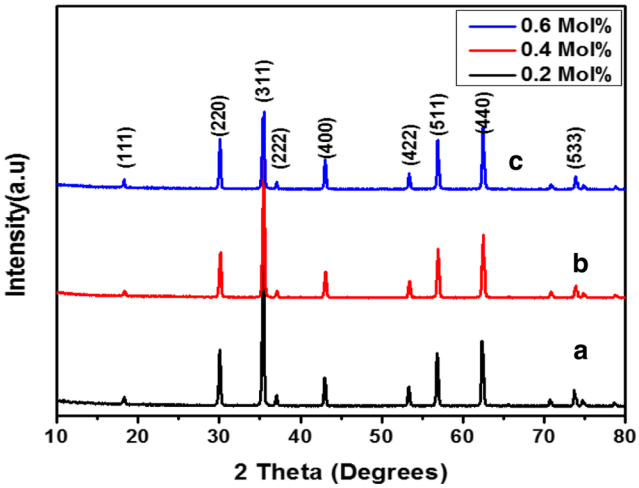

Fig. 1 XRD patterns of (a) 0.2, (b) 0.4, and (c) 0.6 M % Mg-doped $ZnFe_2O_4$ pellets sintered at 1400 °C for 2 h

$$D = \frac{0.94\lambda}{\beta\cos\theta} \quad (1)$$

where D is the average particle, λ is the X-ray wavelength (0.1542 nm), β is the full width at half maximum (FWHM), and θ is the Bragg's angle of the planes. The structural parameters are calculated and tabulated in Table 1.

The variation of the lattice constant depending on the composition is observed in the Fig. 2. Lattice parameter "a" is decreased with increasing Mg content because of the small ionic radius of Mg^{2+} ion [21]. The small sized Mg might occupy interstitial sites, which thereby produces strain within the $ZnFe_2O_4$ [7]. It is observed that peaks shift to higher 2θ value after the addition of Mg. The lattice parameter decreases with increasing Mg content from 8.449 to 8.443 Å, thus obeying Vegard's law. According to Shannon's compilation, the size of the Mg^{2+} (0.79 Å) is smaller than that of the Zn^{2+} ion (0.83 Å) in the unit cell [22]. This contracts the lattice, and hence

Table 1 The structural parameters of Mg-doped $ZnFe_2O_4$ nanoparticles

Composition	2θ (°)	Crystalline size (nm)	Lattice constant (Å)	Grain size (μm)	Structure
0.2 M% Mg	35.19	36.54	8.449	1.63	Cubic
0.4 M% Mg	35.39	27.14	8.447	1.51	Cubic
0.6 M% Mg	35.79	17.78	8.444	1.45	Cubic

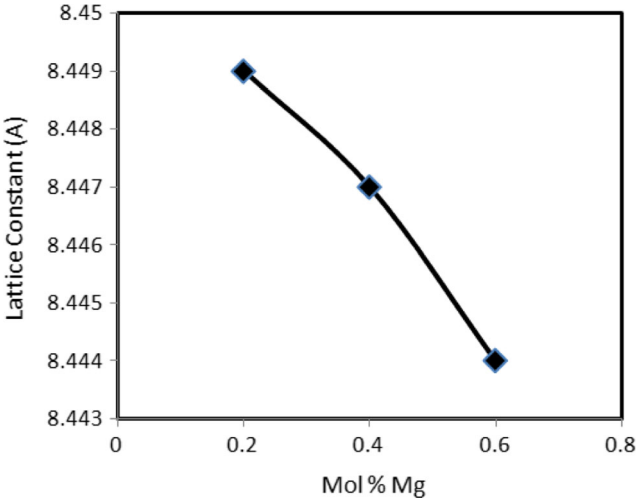

Fig. 2 Variation of lattice constant with mol% of Mg

lattice parameter and volume of the unit cell decrease. The linear decrease in the lattice spacing thus indicates that the Mg ions are replacing the Zn ions in Zn ferrite matrix also indicating that Mg has entered into Zn^{2+} ion sites forming the lattice of spinel ferrite in $Mg_xZn_{1-x}Fe_2O_4$. The diffraction peaks of each Mg-doped samples are sharper and narrower with increasing Mg content indicating that Mg promoted the crystalline growth [23]. Another reason for the observed variation of the lattice parameter is the Jahn–Teller distortion which takes place for Zn^{2+} ions. With increasing Mg^{2+} ion concentration, the Jahn–Teller distortion decreases and the cubic symmetry is increased. Jahn–Teller distortion in the sample may be a compression distortion in the octahedral B site, with increasing Mg^{2+}, the octahedral site returns to its symmetry in the cubic form as confirmed from X-ray [24].

Therefore, the lattice parameters contract when the Mg ion substitutes the Zn ion in the lattice, and the contraction of lattice parameters is a function of Mg content. This is in good agreement with the reduction of the lattice volume. For this reason, it can be concluded that the $Mg_xZn_{1-x}Fe_2O_4$ can form

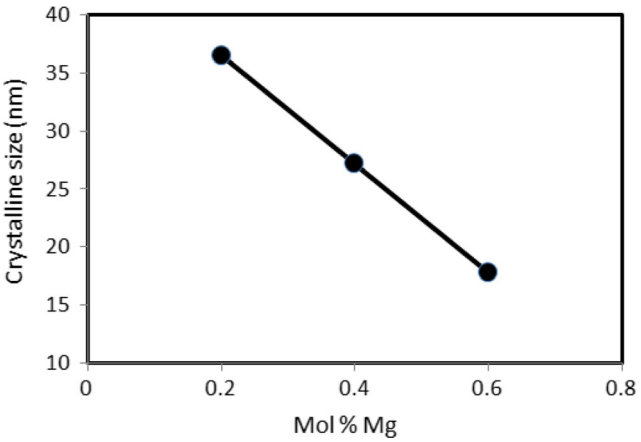

Fig. 3 Variation of crystalline size with mol% of Mg

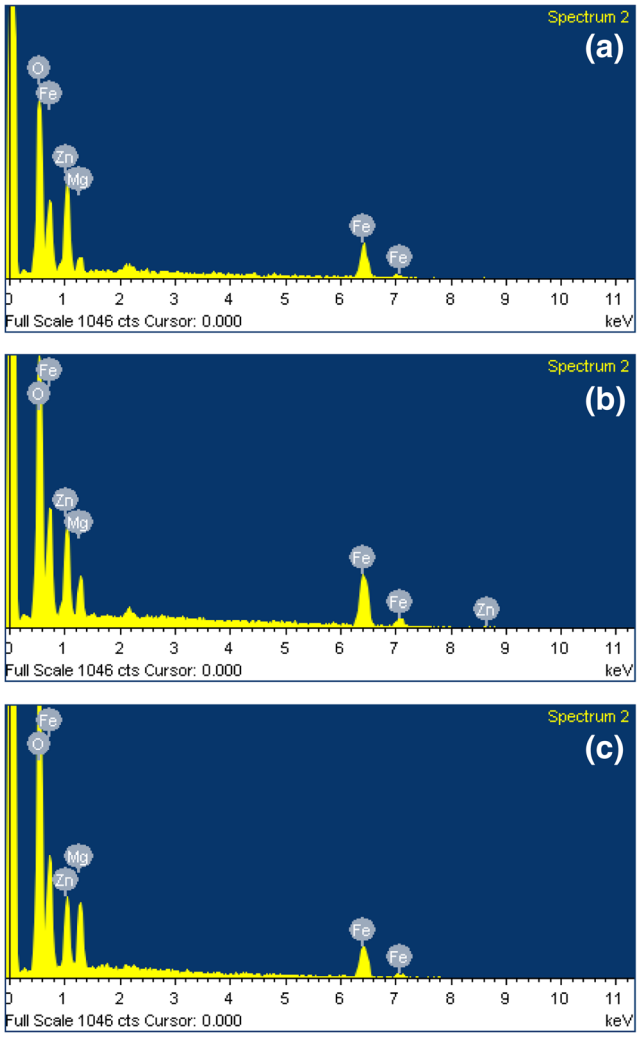

Fig. 4 EDAX spectra of **a** 0.2, **b** 0.4, and **c** 0.6 M% Mg-doped $ZnFe_2O_4$ pellets sintered at 1400 °C for 2 h

in the whole range of Mg content used. The crystallite size decreases with the increase of Mg content. This may be due to the coarsening of the crystal and the growth occurred through the Ostwald ripening mechanism [7, 25]. From the Fig. 3, it is clearly observed that the crystalline size decreases linearly from 36 to 17 nm with an increasing concentration of Mg which indicates that Mg promoted the crystalline growth. The EDAX spectrum shown in Fig. 4 presents the distribution of elements in the composition, and it identifies the presence of Zn, Fe, O, and Mg in all the compositions and placed in Tables 2 and 3.

Table 2 The EDAX analysis of Mg-doped Zn ferrites nanoparticles

Composition	Zn	Fe	O	Mg
0.2 M% Mg	11.67	29.84	55.11	3.38
0.4 M% Mg	8.10	31.07	55.83	4.99
0.6 M% Mg	6.08	29.58	57.13	7.21

Table 3 Elemental analysis of the Mg-doped Zn ferrite sby EDAX

Composition/element	$X = 0.2$		$X = 0.4$		$X = 0.6$	
	Weight (%)	Atomic (%)	Weight (%)	Atomic (%)	Weight (%)	Atomic (%)
O (K)	25.98	55.11	27.24	55.83	29.12	57.13
Mg (K)	2.42	3.38	3.70	4.99	5.59	7.21
Fe (L)	49.12	29.84	52.91	31.07	52.64	29.58
Zn (L)	22.48	11.67	16.15	8.10	12.65	6.08
Total	100.00	100.00	100.00	100.00	100.00	100.00

Surface morphological studies

Figure 5a–c shows the surface morphologies of the sintered pellets of $Mg_xZn_{1-x}Fe_2O_4$ ($x = 0.2$, 0.4, and 0.6); nanoparticles were investigated by the scanning electron microscopy (SEM). The SEM images of $Mg_xZn_{1-x}Fe_2O_4$ samples (Fig. 5a–c) reveal that the entire samples exhibit a compact arrangement of homogeneous nanoparticles with spherical shape and agglomerated with diameter ranging from 30 to 18 nm for Mg-doped Zn ferrite samples. The total surface free energy is reduced with the increase of Mg content. Nanoparticles are agglomerated due to the presence of magnetic interactions among the particles [26–28]. No significant change in morphology is observed with the increase of Mg. Thus, sintering has led to a reduction in grain boundary energy resulting in dense structure.

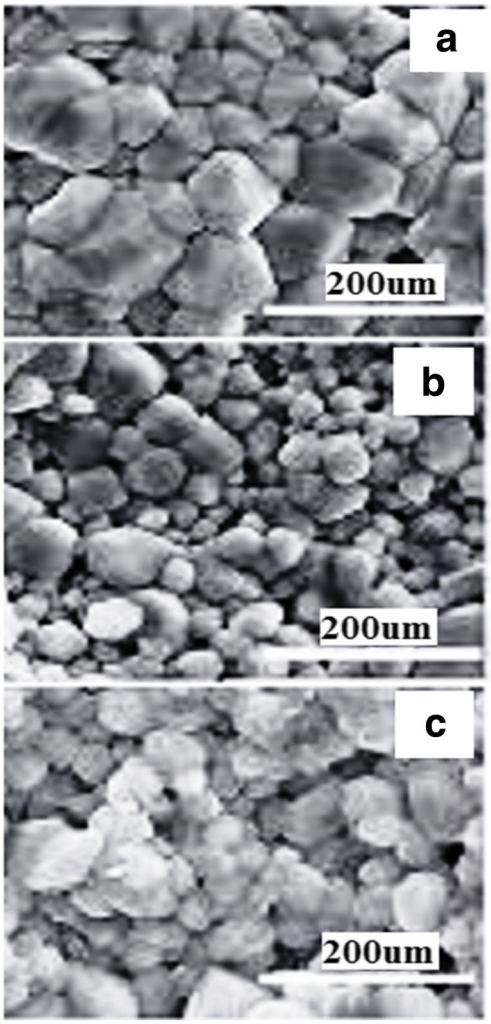

Fig. 5 SEM images of **a** 0.2, **b** 0.4, and **c** 0.6 M% Mg-doped $ZnFe_2O_4$ pellets sintered at 1400 °C for 2 h

The average grain size is measured by using linear intercept method and tabulated in Table 1. The variation of grain size is shown in Fig. 6. From that, we observed that the grain size decreases with the increase of Mg content. This is due to the presence of increased number of pores and also because of smaller grain size, which leads to increased volume fraction of grain boundary. Both the pores and grain boundaries inhibit domain wall movement. However, the decrease in grain size with the increase of Mg content indicates that Mg suppresses the grain growth [29, 30]. Auto-combustion Mg-doped Zn ferrite powders are uniform in both morphology and particle size but are agglomerated to some extent due to interactions between magnetic nanoparticles.

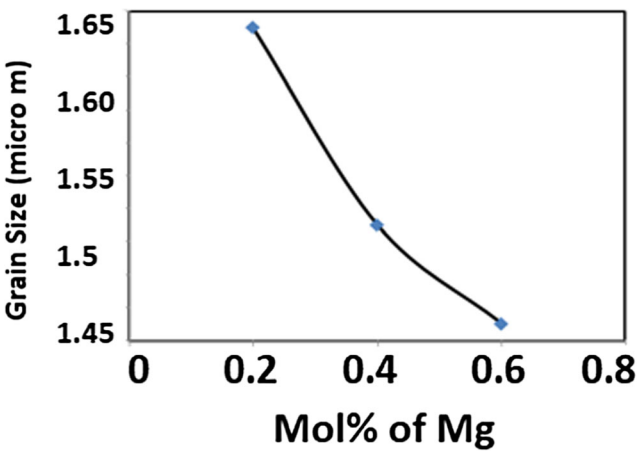

Fig. 6 Variation of grain size with mol% of Mg

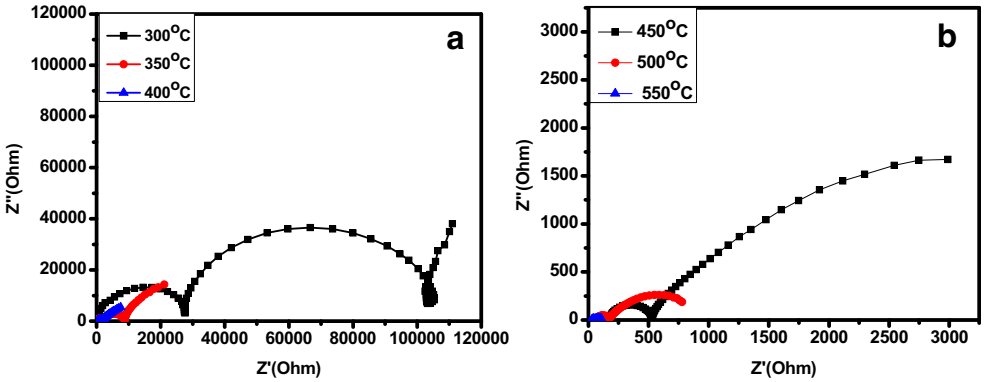

Fig. 7 Impedance spectra of 0.2 M % Mg-doped $ZnFe_2O_4$ nanoparticles at temperatures **a** 300–400 °C and **b** 450–550 °C

Electrical properties

In general, the total conductivity (σ_t) of Mg-doped $ZnFe_2O_4$ nanoparticles is the sum of ionic conductivity (σ_i) and electronic conductivity (σ_e). The contributions by grain, grain boundary, and electrode to the overall ionic conductivity can be estimated by recording ac impedance spectrum. The impedance spectra of sintered samples are recorded at different temperatures and are shown in Figs. 7, 8, and 9. From all these complex plane plots, we observed that two well-separated arcs and portions of a third arc were observed at the lower frequencies for all samples. From this, it is clearly observed that resistivity values decrease by increasing the temperature. The semicircle corresponding to the bulk conductivity is lost from the spectrum above 350 °C. This is caused by the effect of inductances generated within the experimental apparatus on the spectra.

Figure 10 shows comparison of spectra recorded at 450 °C. The spectra show arc at high frequency corresponding to grain interior resistance (R_g). Semicircle at intermediate frequency represents grain boundary resistance (R_{gb}), and tail at low frequency represents electrode contributions and grain resistance. Grain boundary resistance and electrode resistance (R_e) can be estimated from their intercepts on real axis. It has been observed that both R_g and R_{gb} decrease with Mg addition up to 400 °C. Above 400 °C, no drastic change in R_g is observed while R_{gb} still decreases with Mg addition. If Mg is present as the secondary phase within grain, R_g would increase since MgO is insulating. This ultimately indicates formation of Mg-doped $ZnFe_2O_4$ solid solution.

When Mg content increases with a temperature rise, time constants of both grain and grain boundary processes reduce and corresponding resistances decrease. Hence, the conductivity rises with the temperature. The conductivity is then calculated from resistance, thickness l, and cross-section area A, by using the formula [31], $\sigma = l/RA$. The variation of the conductivity at different concentrations of Mg is shown in the Fig. 11. It is observed that conductivity increases with the increase of MgO content. This may be due to the hopping of charge carriers which leads to the increase in the carrier mobility [32]. This trend can be explained with the following Kröger notation equations [30]:

$$Mg^{2+} + Zn^{2+} \rightarrow Mg\left(Zn^{2+}\right) \quad (2)$$

$$2Mg^{2+} + Fe^{3+} \rightarrow 2Mg\left(Fe^{3+}\right) + C.V \quad (3)$$

$$Mg^{2+} + Fe^{3+} \rightarrow Mg_{\Delta} + Fe^{2+} + 1/2O_2 \quad (4)$$

$$Mg^{2+} + 2Zn^{2+} \rightarrow Mg_{\Delta} + 2Zn^{+} \quad (5)$$

$Mg(Zn^{2+})$ and $Mg(Fe^{3+})$ are the divalent ions located in the positions of host zinc and iron oxides in ZnO and Fe_2O_3,

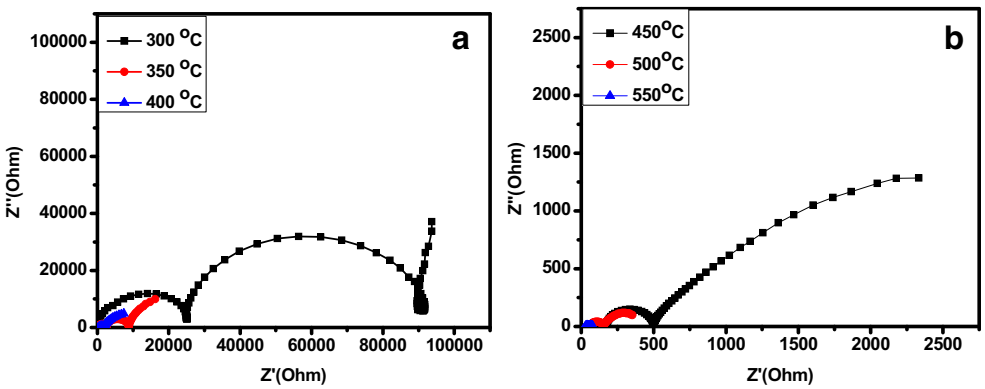

Fig. 8 Impedance spectra of 0.4 M % Mg-doped $ZnFe_2O_4$ nanoparticles at temperatures **a** 300–400 °C and **b** 450–550 °C

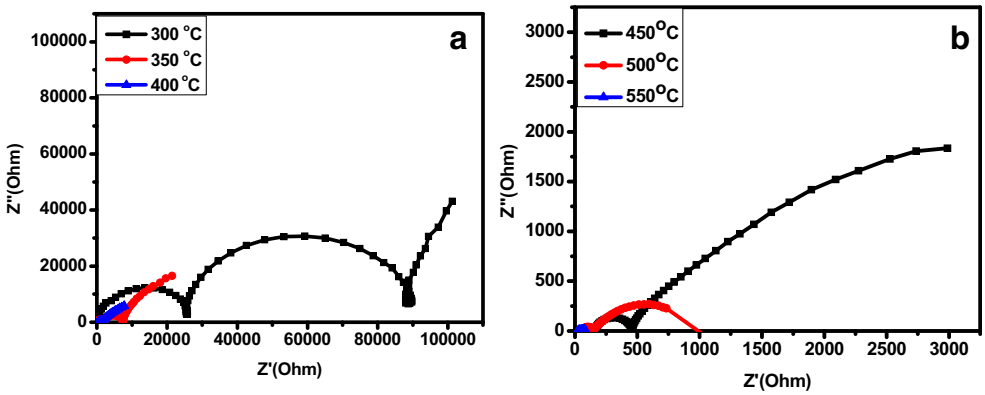

Fig. 9 Impedance spectra of 0.6 M % Mg-doped $ZnFe_2O_4$ nanoparticles at temperatures **a** 300–400 °C and **b** 450–550 °C

respectively [28]; Mg_{Δ} is magnesium ions located in the interstitial positions of zinc and ferric oxide lattices; created cationic (oxygen) vacancies (C.V.). The dissolution of dopant ions in the lattices of reacting oxides according to reaction (2) which led to creation of cationic (oxygen) vacancies might increase the mobility of cations of reacting oxides thus enhancing the ferrite formation. Incorporation of magnesium ions in Fe_2O_3 and ZnO lattices according to reactions (3) and (4) decreased the number of reacting cations (Zn^{2+} and Fe^{3+}) involved in the ferrite formation. So, reaction (2) might be expected to stimulate zinc ferrite formation, while reactions (3) and (4) might exert an opposite effect.

The fact is that MgO doping of Zn/Fe oxides system enhanced zinc ferrite formation suggesting the domination of reaction (2). With the addition of MgO into Zn/Fe oxides system would lead to the formation of oxygen vacancy due to the charge compensation. Mainly electrolyte materials, the vacancy will attract the doping ions to be produced due to complex forces. At lower dopant content, most of these cationic (oxygen) vacancies are probably mobile, which could explain gradual increase of conductivity.

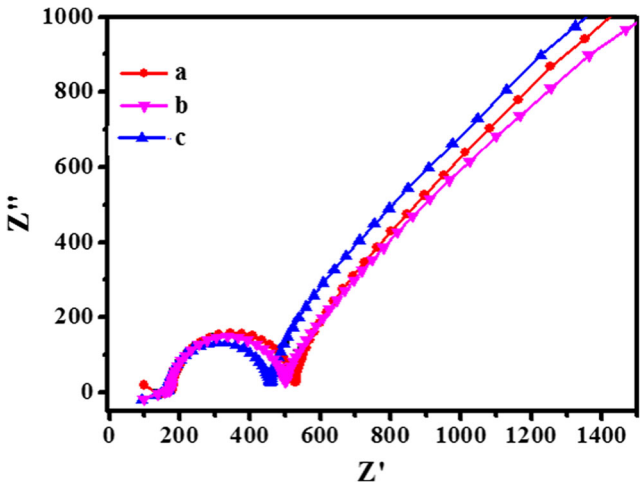

Fig. 10 Nyquist plots of (a) 0.2, (b) 0.4, and (c) 0.6 M % Mg-doped $ZnFe_2O_4$ nanoparticles recorded at 450 °C

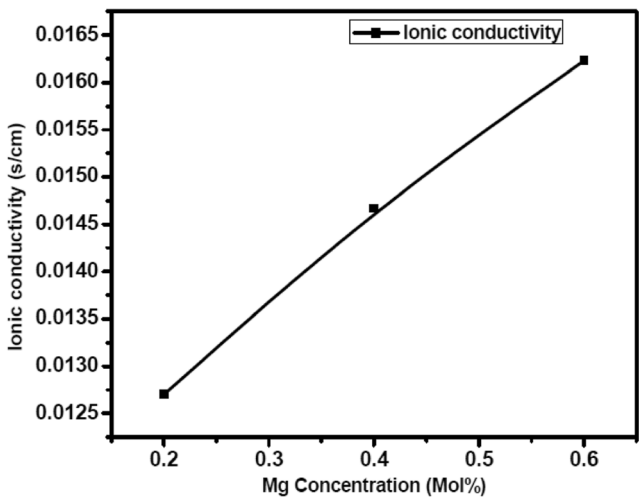

Fig. 11 Variation of ionic conductivity with mol% of Mg

Conclusions

The Mg-doped Zn ferrite nanoparticles are successfully synthesized by auto-combustion method. The XRD study confirms the Mg-doped Zn ferrite nanoparticle has cubic spinel structure. The lattice parameter as well as the crystallite size (from 35.54 to 17.78 nm) decreases with increasing Mg content. No significant change is observed with Mg addition in the morphology of the samples; the grain size decreases from 1.63 to 1.45 μm with the addition of Mg concentration from 0.2 to 0.6 mol%. The ionic conductivity of the Mg-doped Zn ferrite nanoparticles increased with the increase of Mg concentration from 0.012 to 0.0165 s/cm.

References

1. Gimenes, R., Baldissera, M.R., Silva, M.R.A., Silveira, C.A., Soares, D.A.W., Perazolli, L.A., Silva, M.R., Zaghete, M.A.: Structural and magnetic characterization of $Mn_xZn_{1-x}Fe_2O_4$ (x=0.2, 0.35, 0.65, 0.8, 1.0) ferrites obtained by the citrate precursor method. Ceram. Int. **38**, 741–746 (2012)

2. Sharifi, I., Shokrollahi, H., Amiri, S.: Ferrite-based magnetic nanofluids used in hyperthermia applications. J. Magn. Magn. Mater. **324**, 903–915 (2012)
3. Gupta, N., Verma, A., Kashyap, S.C., Dube, D.C.: Microstructural, dielectric and magnetic behavior of spin-deposited nanocrystalline nickel–zinc ferrite thin films for microwave applications. J. Magn. Magn. Mater. **308**, 137–142 (2007)
4. Hajarpour, S., Gheisari, K., Raouf, A.H.: Characterization of nanocrystalline $Mg_{0.6}Zn_{0.4}Fe_2O_4$ soft ferrites synthesized by glycine–nitrate combustion process. J. Magn. Magn. Mater. **329**, 165–169 (2013)
5. Azam, A., Jawad, A., Ahmed, A.S., Chaman, M., Naqvi, A.H.: Structural, optical and transport properties of Al^{3+} doped $BiFeO_3$ nano-powder synthesized by solution combustion method. J. Alloys Compd. **509**, 2909–2913 (2011)
6. Jawad, A., Ahmed, A.S., Ashraf, S.S.Z., Chaman, M., Azam, A.: Exploring the dielectric behaviour of nano-structured Al^{3+} doped $BiFeO_3$ ceramics synthesized by auto ignition process. J. Alloys Compd. **530**, 63–70 (2012)
7. Rahman, S., Nadeem, K., Rehman, M.A., Mumtaz, M., Naeem, S., Papst, I.L.: Structural and magnetic properties of ZnMg-ferrite nanoparticles prepared using the co-precipitation method. Ceram. Int. **39**, 5235–5239 (2013)
8. Sivakumar, M., Takami, T., Ikuta, H., Towata, A., Yasui, K., Tuziuti, T., Kozuka, T., Bhattacharya, D., Iida, Y.: Fabrication of zinc ferrite nanocrystals by sonochemical emulsification and evaporation:observation of magnetization and its relaxation at low temperature. J. Phys. Chem. B. **110**, 15234–15243 (2006)
9. Yang, J.M., Yen, F.S.: Evolution of intermediate phases in the synthesis of zinc ferrite nanopowders prepared by the tartrate precursor method. J Alloys Compd. **450**, 387–394 (2008)
10. Mahavir Singh, J.: A comparative study of the electrical and the magnetic properties and Mössbauer studies of normal and hot pressed $Mg_xMn_{1-x}Fe_2O_4$ ferrites. Magn. Magn. Mater. **299**, 397–403 (2006)
11. Singh, M., Sud, S.P.: Mg–Mn–Al ferrites for high frequency applications. Mod. Phys. Lett. B. **14**, 531–537 (2000)
12. Manjurul Haque, M., Huq, M., Hakim, M.A.: Densification, magnetic and dielectric behaviour of Cu-substituted Mg–Zn ferrites. Mater. Chem. Phys. **112**, 580–586 (2008)
13. Jordan, A., Wust, P., Scholz, R.: Scientific and clinical applications of magnetic carriers, pp. 569–595. Plenum Press, New York (1997)
14. Robert, R., Greenberg, P.B., Elisabete, A., De Fernandes, N.: Neutron activation analysis: a primary method of measurement. Spectrochim. Acta Part B. **66**, 193–241 (2011)
15. Skołyszewska, B., Tokarz, W., Przybylski, K., Kakol, Z.: Preparation and magnetic properties of Mg Zn and MnZn ferrites. Physica C. **387**, 290–294 (2003)
16. Rezlescu, E., Sachelarie, L., Rezlescu, N.: Influence of copper ions on the structure and electromagnetic properties of Mg-Zn ferrite. J. Optoelectron. Adv. Mater. **8**, 1019–1022 (2006)
17. Nadeem, K., Rahman, S., Mumtaz, M.: Effect of annealing on properties of Mg doped Zn-ferrite nanoparticles. Prog. Nat. Sci: Mater. Int. **25**, 111–116 (2015)
18. Rafiq, M.A., Khan, M.A., Asghar, M., Ilyas, S.Z., Shakir, I., Shahid, M., Warsi, M.F.: Influence of Co^{2+} on structural and electromagnetic properties of Mg–Zn nanocrystals synthesized via co-precipitation route. Ceram. Int. **41**, 10501–10505 (2015)
19. Manikandan, A., Vijaya, J.J., Sundararajan, M., Meganathan, C., Kennedy, L.J., Bououdina, M.: Optical and magnetic properties of Mg-doped $ZnFe_2O_4$ nanoparticles prepared by rapid microwave combustion method. Super Lattices Microstruct. **64**, 118–131 (2013)
20. Kumar, A.G.S., Sarmash, T.S., Obulapathi, L., Rani, D.J., Rao, T.S., Asokan, K.: Structural, optical and electrical properties of heavy ion irradiated CdZnO thin films. Thin. Solid Films. **605**, 102–107 (2016)
21. Manikandan, A., Vijaya, J.J., Kennedy, L.J., Bououdina, M.: Structural, optical and magnetic properties of $Zn_{1-x}Cu_xFe_2O_4$ nanoparticles prepared by microwave combustion method. J. Mol. Struct. **1035**, 332–340 (2013)
22. Salah, L.M., Moustafa, A.M., Farag, I.S.A.: Structural characteristics and electrical properties of copper doped manganese ferrite. Ceram. Int. **38**, 5605–5611 (2012)
23. Prabu, J.H., Johnson, I.: Greener cum chemical synthesis and characterization of Mg doped ZnS nanoparticles and their engineering band gap performance. Int. J. Engeg. Res. Appl. **5**, 99–105 (2015)
24. Ateia, E., Ahmed, M.A., Ghouniem, R.M.: Electrical properties and initial permeability of CueMg ferrites. Solid State Sci. **31**, 99–106 (2014)
25. Li, S., Wu, Z., Li, W., Liu, Y., Zhuo, R., Yan, D., Jun, W., Yan, P.: One-pot synthesis of ZnS hollow spheres via a low temperature, template-free hydrothermal route. Cryst. Eng. Comm. **15**, 1571–1577 (2013)
26. Luo, F., Yan, C.H.: Anti-phase boundaries pinned abnormal positive magnetoresistance in Mg doped nanocrystalline zinc spinel ferrite. Chem. Phys. Lett. **452**, 296–300 (2008)
27. Alarifi, A., Deraz, N.M., Shaban, S.: Structural, morphological and magnetic properties of $NiFe_2O_4$ nano-particles. J. Alloy Compd. **486**, 501–506 (2009)
28. Deraz, N.M., Alarifi, A.: Fabrication and characterization of pure and doped Zn/Fe nanocomposites. Int. J. Electrochem. Sci. **7**, 3809–3816 (2012)
29. Berchmans, L.J., Selvan, R.K., Kumar, P.N.S., Augustin, C.O.: Structural and electrical properties of $Ni_{1-x}Mg_xFe_2O_4$ synthesized by citrate gel process. J. Magn. Magn. Mater. **279**, 103–110 (2004)
30. Kröger, F.A.: Chemistry of imperfect crystals. North-Holland, Amsterdam (1964)
31. Rani, D.J., Kumar, A.G.S., Rao, T.S.: Substrate temperature-dependent physical properties of nanocrystalline zirconium titanate thin films. J. Coat. Technol. Res. **14**(5), 971–980 (2017)
32. Ponpandian, N., Balaya, P., Narayanasamy, A.: Electrical conductivity and dielectric behaviour of nanocrystalline $NiFe_2O_4$ spinel. J. Phys. Condens. Matter. **14**, 3221–3237 (2002)